Graph Neural Network Guided Selection of Functional Polymers for Charge Transfer Doping of 2D Materials

Fabia Farlin Athena[†§*] **Tara Peña**[†*] **Kalee Francis Rozylowicz**[‡*] **Anh Tuan Hoang**[‡]
Andrew J. Mannix[‡] **H.-S. Philip Wong**[†] **Eric Pop**[†] **Alberto Salleo**[‡]
[†]Department of Electrical Engineering, Stanford University
[‡]Department of Materials Science and Engineering, Stanford University
[§]fathena@stanford.edu

Abstract

Two-dimensional (2D) semiconductors are competing materials for post-Si transistors because of their desirable carrier mobilities and band gaps with atomic thinness. However, high contact resistances plague the performance of 2D-based devices. Thus, non-destructive doping strategies are needed in order to overcome this challenge for complementary (n-type and p-type) 2D logic. Here, we present the use of functional polymers to non-destructively introduce charge transfer n-type and p-type doping in 2D materials. First, we utilize a multitask graph neural network (GNN), trained on density functional theory-calculated properties, to predict properties like ionization energy and electron affinity of candidate polymers. These predictions are then used to select polymers capable of doping n-type and p-type monolayer MoS_2 and WSe_2 based on band-level alignment criteria. We validate our screening strategy with Raman spectroscopy, confirming successful p-type doping of WSe_2 with PEDOT:PSS and Nafion, and n-type doping of MoS_2 with PEI and WSe_2 with p(gPyDPP-MeOT2). The results demonstrate a practical model-to-lab pipeline that effectively narrows the search space for polymer dopants, bridging high-throughput computational materials screening with experimental validation.

1 Introduction

Monolayer transition metal dichalcogenides (TMDs), such as MoS_2 and WSe_2, are promising materials for next-generation electronics [1, 2], but their performance is often limited by large contact resistances [3]. Fermi-level pinning occurs closest to the conduction band edge in these materials, resulting in larger p-type contact resistances in 2D transistors [4–6]. Traditional doping techniques like ion implantation or substitutional doping inherently entail modifying the lattice, thus often deteriorating the quality of 2D semiconductors. A promising alternative is charge-transfer doping [7], since this method can preserve the quality of the 2D lattice. This method simply consists of engineering the band alignment between a capping layer with that of the TMD [7–9], where electrons or holes can be transferred across the van der Waals interface. While recent works have found molecular doping [10] and charge-transfer doping with solvents to successfully dope p-type WSe_2 transistors [11], there remain challenges with temperature or time stability of the doping state.

Another underexplored route is simply encapsulating 2D device channels with functional polymers [12, 13], where this presents non-destructive options to achieve both n-type and p-type charge-transfer doping for 2D materials. The chemical space of potential polymer dopants is immense, thus allowing for a large volume of opportunity while simultaneously making exhaustive experimental screening impractical. Polymer informatics, particularly the use of GNNs, offers a powerful tool to

[*]Equal contribution.

AI4Mat Workshop at the 39th Conference on Neural Information Processing Systems (NeurIPS 2025).

navigate this space by learning structure-property relationships [14–17]. By training GNNs on large datasets of polymer properties [18–20], we can rapidly predict the electronic characteristics relevant for successful charge transfer doping.

Here, we present a compact workflow that leverages a multitask GNN, polyGNN [16], to screen for effective polymer dopants for MoS_2 and WSe_2. We translate the GNN's predictions of fundamental electronic properties into an approximate polymer work function, which serves as a key descriptor for our screening. We establish explicit energy alignment criteria for achieving both n-type and p-type doping. Finally, we connect our computational screen to laboratory experiments by performing Raman spectroscopy on selected polymer/TMD heterostructures, demonstrating the viability of our AI-guided approach.

2 Methodology

2.1 Computational Screening with GNN

Our screening framework is built upon polyGNN, a multitask GNN architecture designed for predicting a wide range of polymer properties [16]. We used the publicly released pretrained weights of polyGNN, which was trained on 13,388 polymers with 36 properties spanning thermal, thermodynamic/physical, electronic, optical/dielectric, mechanical, solubility, and gas permeability. The labels used came from a mix of in-house density functional theory (DFT) computations and curated external experimental sources. The encoder constructs periodic polymer graphs and, together with data augmentation, provides invariance to repeat-unit choices. We utilize the repeat-unit Simplified Molecular Input Line Entry System (SMILES) [21] for each candidate polymer and read the ensemble mean and standard deviation of the predicted properties. For this work, we utilize polyGNN's ability to predict two key electronic properties: the vertical Ionization Energy (IE) and Electron Affinity (EA). In the polyGNN corpus, the IE and EA labels are derived from DFT calculations.

From Predicted Properties to Work Function. To assess a polymer's doping potential, we must relate its predicted properties to the vacuum-referenced energy levels used in device physics. IE is the energy required to remove an electron from a neutral molecule. It corresponds to the energy of the Highest Occupied Molecular Orbital (HOMO) relative to the vacuum level: $\mathrm{E}_{\mathrm{HOMO}}^{\mathrm{vac}} = -\mathrm{IE}$. EA is the energy released when an electron is added to a neutral molecule. It corresponds to the energy of the Lowest Unoccupied Molecular Orbital (LUMO): $\mathrm{E}_{\mathrm{LUMO}}^{\mathrm{vac}} = -\mathrm{EA}$.

For an efficient first-pass screen, we approximate the polymer's work function (WF) as the energy difference from vacuum level to its mid-gap energy, calculated directly from the polyGNN predictions: $\mathrm{WF} \simeq \frac{1}{2}(\mathrm{IE} + \mathrm{EA})$. This process allows us to quickly assess whether a polymer is likely to donate or accept electrons when interfaced with a TMD. This simplification does not apply to extrinsically doped polymer semiconductors such as PEDOT:PSS, where heavy p-type doping positions the Fermi level near the HOMO. In such cases, the IE provides a more appropriate descriptor of charge transfer behavior, since it reflects the energy required to remove an electron from the already oxidized polymer.

Charge-Transfer Doping Criteria. Effective charge transfer is governed by the energy alignment between the polymer and the TMD. We apply two distinct, physically-grounded criteria for n-type and p-type screening:

- **n-type Doping:** Requires the polymer's Fermi level ($\mathrm{E_F}$) to be *above* the TMD's Conduction Band Minimum (CBM). For a first-pass screen of neutral polymers, we approximate the polymer's $\mathrm{E_F}$ using its mid-gap energy (our calculated WF). The criterion is $\mathrm{WF} < -\mathrm{E_{CBM}}$.
- **p-type Doping:** Requires the polymer to have occupied states (i.e., its HOMO) *below* the TMD's Valence Band Maximum (VBM). This allows the polymer to accept an electron from the TMD. The most direct physical descriptor for this is the polymer's IE. The criterion is $\mathrm{E}_{\mathrm{HOMO}}^{\mathrm{vac}} < \mathrm{E_{VBM}}$, which translates to $\mathrm{IE} > -\mathrm{E_{VBM}}$.

For MoS_2, the CBM is $\sim -3.84\,\mathrm{eV}$ and the VBM is $\sim -6.32\,\mathrm{eV}$ [9]. Thus, n-type dopant (electron donation) requires polymer $\mathrm{WF} < 3.84\,\mathrm{eV}$ and p-type dopant (electron acceptance) requires polymer $\mathrm{IE} > 6.32\,\mathrm{eV}$. For WSe_2, the CBM is $\sim -3.53\,\mathrm{eV}$ and the VBM is $\sim -5.61\,\mathrm{eV}$ [9]. Thus, n-type dopant (electron donation) requires polymer $\mathrm{WF} < 3.53\,\mathrm{eV}$ and p-type dopant (electron acceptance) requires polymer $\mathrm{IE} > 5.61\,\mathrm{eV}$.

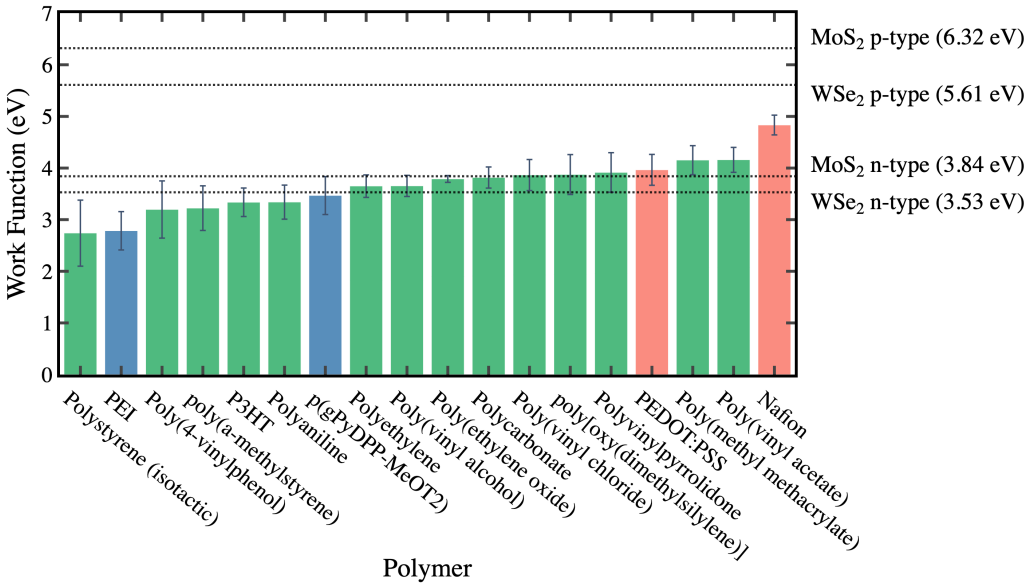

Figure 1: Work functions of various functional polymers predicted by the polyGNN model. Error bars represent the propagated standard deviation from the GNN predictions. Horizontal dotted lines indicate the n-type WF thresholds. P-type screening is assessed via IE (see Sec. 2.1 and Fig. 6), not directly from this WF plot. Polymers validated experimentally are highlighted: PEDOT:PSS and Nafion (highlighted in red for p-type validation), PEI and DPP (in blue for n-type validation).

The band edges we implement for these criteria are from previous work that examines first-principles calculations of perfect monolayer TMD films with no substrate [9]. We note that different simulation approaches will lead to variations in the extracted band alignments and band gaps [14]. We chose the following criterion based on how well it aligns with band gap values determined by experimental scanning tunneling microscopy on monolayer TMDs [22], although these experimental values are subject to variation from dielectric environment, strain, and/or disorder [23].

2.2 Experimental Validation via Raman Spectroscopy

To verify the doping effects predicted by our screening, we fabricated heterostructures by depositing selected polymers onto monolayer MoS_2 and WSe_2 grown via solid-source chemical vapor deposition [24], with growth conditions detailed in Appendix A.4. We then performed Raman spectroscopy, a rapid non-destructive technique for probing strain, doping, and disorder in TMDs. Changes in carrier concentration alter the lattice vibrations, leading to characteristic shifts in the positions and intensities of Raman-active phonon modes (e.g., the A_1' mode in TMDs) [25, 26]. By comparing the Raman spectra of the pristine and polymer-coated TMDs, we can confirm the presence and type (n-type or p-type) of doping.

3 Results and Discussion

3.1 GNN-based Screening of Polymer Dopants

We applied our polyGNN-based workflow to screen a library of polymers. Figure 1 shows the predicted work functions for a representative set of candidates, benchmarked against the doping thresholds for MoS_2 and WSe_2. The model identifies polymers spanning a wide range of work functions, from potential n-type dopants with low WFs (e.g., PEI) to materials with high WFs (e.g., Nafion). This screening plot serves as a direct guide for experimental efforts. It allows us to not only identify candidates that strictly satisfy the doping criteria but also to rank and prioritize the most promising polymers when ideal candidates are scarce. This ability to rapidly prioritize candidates saves significant experimental time and resources.

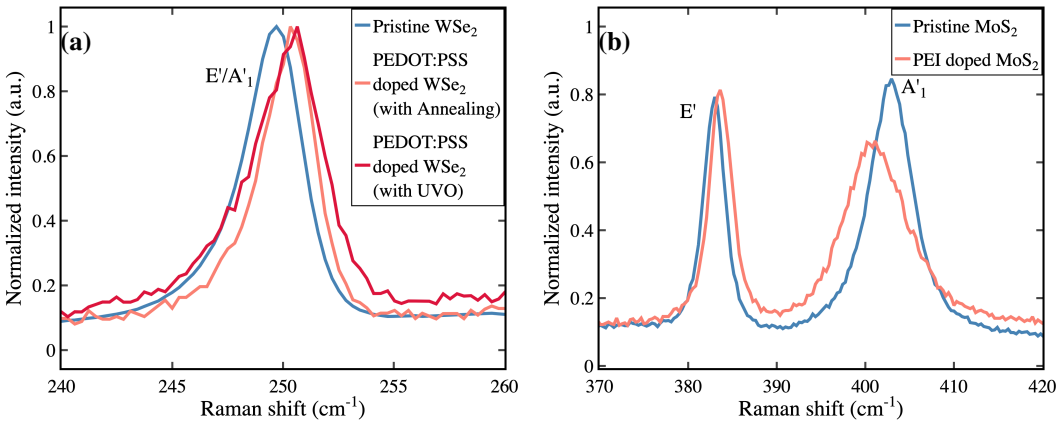

Figure 2: Experimental validation of polymer doping using Raman spectroscopy. (a) Spectrum of monolayer WSe_2 before (blue) and after (red) coating with the p-type dopant PEDOT:PSS. The peak shift to the right confirms withdrawal of electrons [26]. (b) Spectrum of monolayer MoS_2 before (blue) and after (red) coating with the n-type dopant PEI. The A_1' peak shift to the left, intensity changes, and increase in the peak width are clear signatures of electron injection [25].

3.2 Experimental Verification of Doping

We performed Raman spectroscopy on four polymer/TMD systems to validate our screening approach. The results demonstrate how the GNN-based ranking successfully guides the selection of both n-type and p-type dopants.

p-type Doping of WSe_2. As defined in our methodology (Sec. 2.1), effective hole injection into WSe_2 requires the polymer's IE $> 5.61\,\text{eV}$. Our initial screen based on the mid-gap work function (WF) did not identify any polymers that met the WF $> 5.61\,\text{eV}$ criterion. However, examining the predicted IEs directly (our defined criterion for p-doping) provides a clearer and more accurate picture, as shown in Appendix Figure 6. This analysis reveals precisely why our top-ranked candidates were successful experimentally:

- **Nafion:** The model predicts an exceptionally high IE of $\sim 8.62 \pm 0.33$ eV. This value is well above the $5.61\,\text{eV}$ threshold, positioning its HOMO level ideally for strong electron acceptance from WSe_2. This prediction strongly aligns with the experimental observation of p-type doping shown in Appendix Figure 4.
- **PEDOT:PSS:** The predicted IE of $\sim 5.36 \pm 0.42$ eV is slightly below the theoretical threshold for hole injection into WSe_2, yet consistent with the model's predictive uncertainty. This result aligns with its observed effectiveness as a p-type dopant, which we confirmed using Raman spectroscopy in Figure 2(a).

The success of these polymers, correctly identified by analyzing their HOMO levels, underscores the importance of using the most direct physical descriptors for screening. While the simplified work function metric is useful for a general ranking, the predicted IE is a more crucial and accurate indicator for selecting p-type dopants.

n-type Doping of MoS_2 and WSe_2. In contrast to the p-doping case, the GNN screen identified multiple polymers that clearly satisfied the criteria for n-type doping.

- **PEI on MoS_2:** The predicted WF of $\sim 2.78 \pm 0.37$ eV is well within the $< 3.84\,\text{eV}$ requirement for n-doping MoS_2. The Raman data in Figure 2(b) directly confirm this prediction, showing distinct signatures of n-type doping.
- **p(gPyDPP-MeOT2) (DPP) on WSe_2:** The DPP polymer's predicted WF of $\sim 3.47 \pm 0.36$ eV also comfortably meets the $< 3.53\,\text{eV}$ threshold for n-doping WSe_2. Again, the experimental Raman spectra in Appendix Figure 5 validate the GNN's prediction, indicating that the polymer behaves as an n-type dopant.

These results underscore the value of this GNN-based screening approach. It successfully identifies n-type dopants that fall within the expected windows under vacuum-level alignment assumptions and effectively prioritizes the best available candidates for the more challenging p-type doping task. The framework thus provides a robust and nuanced guide for experimental materials selection.

4 Conclusion

We have demonstrated a practical workflow that integrates a multitask polymer GNN with experimental validation to accelerate the discovery of functional polymer dopants for 2D materials. By translating polyGNN's predictions into an approximate work function, we created a rapid screening tool that successfully identified viable candidates for both n-type and p-type doping. Raman spectroscopy on four polymer/TMD systems confirmed the predictions for n-dopants (PEI and DPP) and validated our ranking-based selection of p-dopants (PEDOT:PSS and Nafion).

This work establishes a robust model-to-lab pipeline where computational screening effectively guides experimental efforts. Future work should focus on refining the models to account for solid-state and interfacial effects, for instance by incorporating image-charge corrections or training on data from thin-film measurements (e.g., ultraviolet photoelectron spectroscopy), to further improve predictive accuracy and bridge the gap between idealized models and real-world device performance.

5 Acknowledgment

Supported in part by SRC JUMP 2.0 PRISM and CHIMES Center, Stanford Differentiated Access Memory, SystemX Alliance, NMTRI. F.F.A. would like to thank the support from the Stanford Energy Postdoctoral Fellowship and Precourt Institute for Energy. T.P. acknowledges the NSF MPS-Ascend postdoctoral fellowship.

References

[1] Kevin P O'Brien, Carl H Naylor, Chelsey Dorow, Kirby Maxey, Ashish Verma Penumatcha, Andrey Vyatskikh, Ting Zhong, Ande Kitamura, Sudarat Lee, Carly Rogan, et al. Process integration and future outlook of 2D transistors. *Nature Communications*, 14(1):6400, 2023.

[2] Yuan Liu, Xidong Duan, Hyeon-Jin Shin, Seongjun Park, Yu Huang, and Xiangfeng Duan. Promises and prospects of two-dimensional transistors. *Nature*, 591(7848):43–53, 2021.

[3] Xiankun Zhang, Zhuo Kang, Li Gao, Baishan Liu, Huihui Yu, Qingliang Liao, Zheng Zhang, and Yue Zhang. Molecule-upgraded van der waals contacts for schottky-barrier-free electronics. *Advanced Materials*, 33(45):2104935, 2021.

[4] Daisuke Kiriya, Mahmut Tosun, Peida Zhao, Jeong Seuk Kang, and Ali Javey. Air-stable surface charge transfer doping of MoS_2 by benzyl viologen. *Journal of the American Chemical Society*, 136(22):7853–7856, 2014.

[5] Namphung Peimyoo, Weihuang Yang, Jingzhi Shang, Xiaonan Shen, Yanlong Wang, and Ting Yu. Chemically driven tunable light emission of charged and neutral excitons in monolayer WS_2. *ACS Nano*, 8(11):11320–11329, 2014. doi: 10.1021/nn504196n.

[6] Zexin Li, Dongyan Li, Haoyun Wang, X. Xu, L. Pi, P. Chen, T. Zhai, and X. Zhou. Universal p-type doping via lewis acid for 2D transition-metal dichalcogenides. *ACS Nano*, 16(3):4884–4891, 2022. doi: 10.1021/acsnano.2c00513.

[7] Connor J McClellan, Eilam Yalon, Kirby KH Smithe, Saurabh V Suryavanshi, and Eric Pop. High current density in monolayer MoS_2 doped by AlO_x. *ACS nano*, 15(1):1587–1596, 2021.

[8] Heather M. Hill, Albert F. Rigosi, Kwang Taeg Rim, George W. Flynn, and Tony F. Heinz. Band alignment in MoS_2/WS_2 transition metal dichalcogenide heterostructures probed by scanning tunneling microscopy and spectroscopy. *Nano Letters*, 16(8):4831–4837, 2016. doi: 10.1021/acs.nanolett.6b01007.

[9] Filip A. Rasmussen and Kristian S. Thygesen. Computational 2D materials database: Electronic structure of transition-metal dichalcogenides and oxides. *The Journal of Physical Chemistry C*, 119(23):13169–13183, 2015. doi: 10.1021/acs.jpcc.5b02950.

[10] Hao-Yu Lan, Chih-Pin Lin, Lina Liu, Jun Cai, Zheng Sun, Peng Wu, Yuanqiu Tan, Shao-Heng Yang, Tuo-Hung Hou, Joerg Appenzeller, et al. Uncovering the doping mechanism of nitric oxide in high-performance p-type WSe_2 transistors. *Nature Communications*, 16(1):4160, 2025.

[11] Lauren Hoang, Robert K. A. Bennett, Anh Tuan Hoang, Tara Pena, Zhepeng Zhang, Marisa Hocking, Ashley P. Saunders, Fang Liu, Eric Pop, and Andrew J. Mannix. Low resistance p-type contacts to monolayer WSe_2 through chlorinated solvent doping. *arXiv preprint arXiv:2504.21102*, 2025.

[12] Hans He, Kyung Ho Kim, Andrey Danilov, Domenico Montemurro, Liyang Yu, Yung Woo Park, Floriana Lombardi, Thilo Bauch, Kasper Moth-Poulsen, Tihomir Iakimov, et al. Uniform doping of graphene close to the dirac point by polymer-assisted assembly of molecular dopants. *Nature Communications*, 9(1):3956, 2018.

[13] Tien Dat Ngo, Myeongjin Lee, Zheng Yang, Fida Ali, Inyong Moon, and Won Jong Yoo. Control of the schottky barrier and contact resistance at metal–WSe_2 interfaces by polymeric doping. *Advanced Electronic Materials*, 6(10):2000616, 2020.

[14] Yufeng Liang, Shouting Huang, Ryan Soklaski, and Li Yang. Quasiparticle band-edge energy and band offsets of monolayer of molybdenum and tungsten chalcogenides. *Applied Physics Letters*, 103(4):042106, 2013. doi: 10.1063/1.4816517.

[15] Ming-Hui Chiu, Chendong Zhang, Hung Wei Shiu, Chang-Hsiao Chuu, Chih-Yuan S. Chen, Chia-Hao Chen, Mei-Yin Chou, Chih-Kang Shih, and Lain-Jong Li. Determination of band alignment in the single-layer MoS_2/WSe_2 heterojunction. *Nature Communications*, 6:7666, 2015. doi: 10.1038/ncomms8666.

[16] Rishi Gurnani, Christopher Kuenneth, Aubrey Toland, and Rampi Ramprasad. Polymer informatics at scale with multitask graph neural networks. *Chemistry of Materials*, 35(4):1560–1567, 2023.

[17] Matteo Aldeghi and Connor W Coley. A graph representation of molecular ensembles for polymer property prediction. *Chemical Science*, 13(35):10486–10498, 2022.

[18] Rohit Batra, Le Song, and Rampi Ramprasad. Emerging materials intelligence ecosystems propelled by machine learning. *Nature Reviews Materials*, 6(8):655–678, 2021.

[19] Huan Doan Tran, Chiho Kim, Lihua Chen, Anand Chandrasekaran, Rohit Batra, Shruti Venkatram, Deepak Kamal, Jordan P Lightstone, Rishi Gurnani, Pranav Shetty, et al. Machine-learning predictions of polymer properties with polymer genome. *Journal of Applied Physics*, 128(17), 2020.

[20] Chiho Kim, Anand Chandrasekaran, Tran Doan Huan, Deya Das, and Rampi Ramprasad. Polymer genome: a data-powered polymer informatics platform for property predictions. *The Journal of Physical Chemistry C*, 122(31):17575–17585, 2018.

[21] David Weininger. Smiles, a chemical language and information system. 1. introduction to methodology and encoding rules. *Journal of chemical information and computer sciences*, 28 (1):31–36, 1988.

[22] Dian Li, Xiong Wang, Xiaoyong Mo, Edmund C. M. Tse, and Xiaodong Cui. Electronic gap characterization at mesoscopic scale via scanning probe microscopy under ambient conditions. *Nature Communications*, 13(4648):1–7, 2022.

[23] Daniel Rhodes, Sang Hoon Chae, Rebeca Ribeiro-Palau, and James Hone. Disorder in van der waals heterostructures of 2D materials. *Nature Materials*, 18:541–549, 2019.

[24] Kirby KH Smithe, Chris D English, Saurabh V Suryavanshi, and Eric Pop. Intrinsic electrical transport and performance projections of synthetic monolayer MoS_2 devices. *2D Materials*, 4 (1):011009, 2016.

[25] Biswanath Chakraborty, Achintya Bera, DVS Muthu, Somnath Bhowmick, Umesh V Waghmare, and AK Sood. Symmetry-dependent phonon renormalization in monolayer MoS_2 transistor. *Physical Review B—Condensed Matter and Materials Physics*, 85(16):161403, 2012.

[26] Thibault Sohier, Evgeniy Ponomarev, Marco Gibertini, Helmuth Berger, Nicola Marzari, Nicolas Ubrig, and Alberto F Morpurgo. Enhanced electron-phonon interaction in multivalley materials. *Physical Review X*, 9(3):031019, 2019.

A Appendix

A.1 Optical micrograph

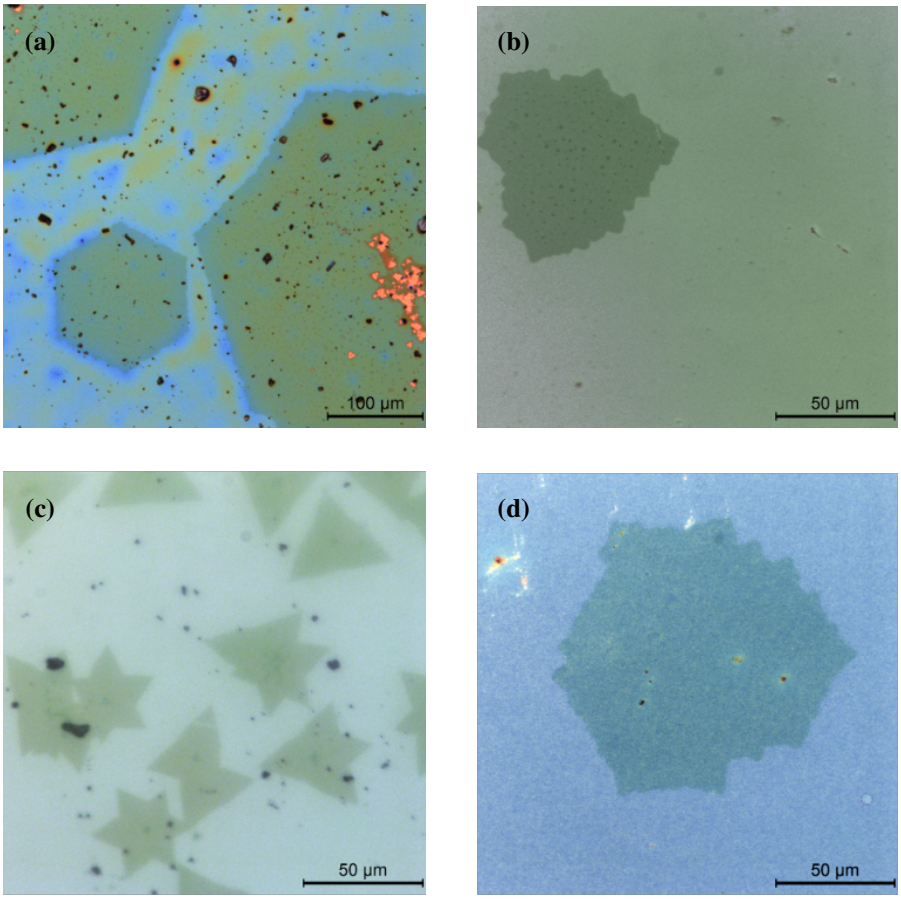

Figure 3: (a) Optical micrograph of WSe_2 coated with the conjugated polymer PEDOT:PSS; (b) WSe_2 coated with Nafion; (c) MoS_2 coated with PEI; and (d) WSe_2 coated with DPP. In all cases, the polymer-coated 2D material exhibits a uniform coating.

A.2 Additional Experimental Raman Data

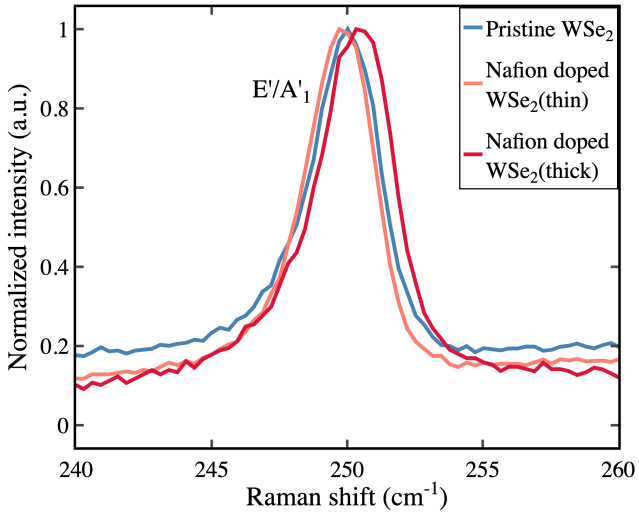

Figure 4: Raman spectra of WSe_2 before and after coating with Nafion. The observed peak shifts are consistent with p-type doping, which aligns with the predictions for Nafion by the GNN model (see Figure 6).

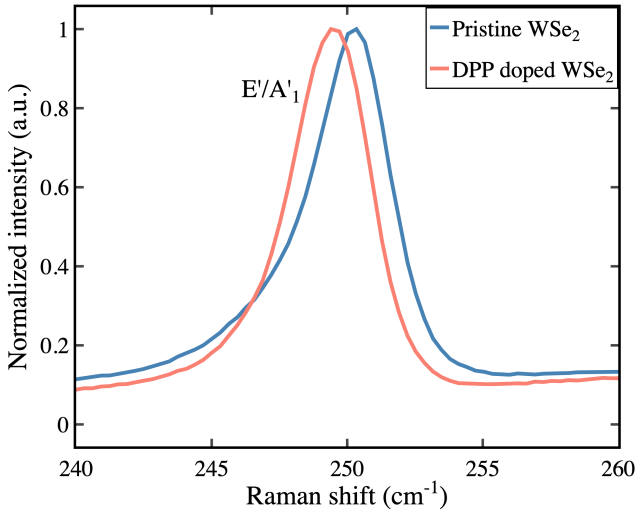

Figure 5: Raman spectra of WSe_2 before and after doping with the polymer DPP. The spectral changes indicate n-type doping behavior. The measured doping type aligns perfectly with the prediction from polyGNN.

A.3 HOMO from GNN

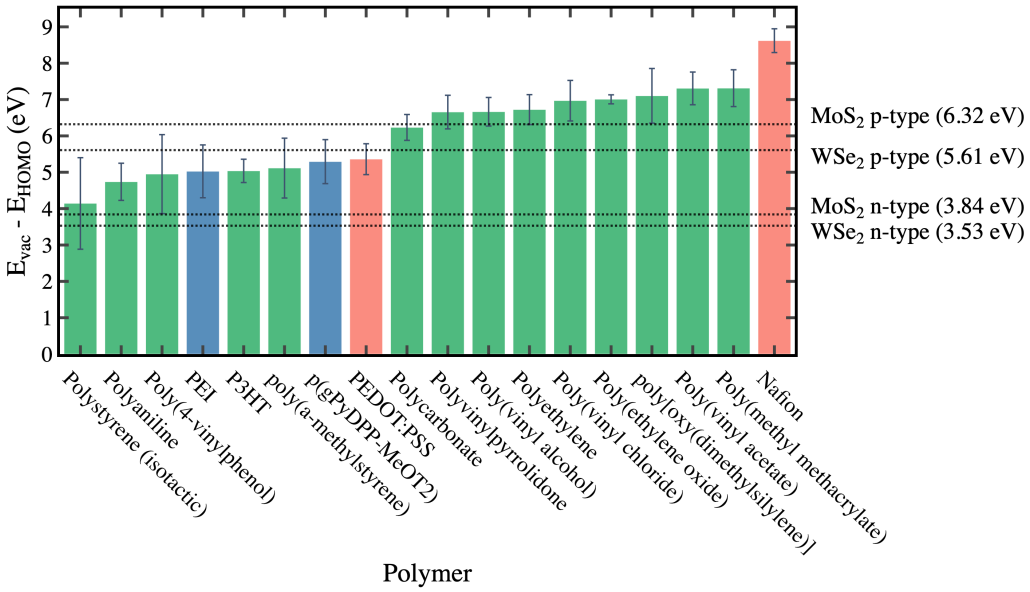

Figure 6: GNN-predicted ionization energies for selected polymers. The ionization energy corresponds to the energy of the HOMO level relative to vacuum (E_{vac}-E_{HOMO}). Error bars represent the standard deviation of the GNN model's predictions. Dashed lines indicate the VBM and CBM of WSe_2 and MoS_2. VBM lines serve as the energy thresholds for effective p-type doping.

A.4 Growth of MoS_2 and WSe_2

The MoS_2 and WSe_2 crystals were grown using a two-zone solid source chemical vapor deposition (SS-CVD) method. Thermally-oxidized amorphous SiO_2 on Si was used as the substrate, and typically underwent a hexamethyldisilazane (HMDS) vapor prime before growth. Perylene-3,4,9,10-tetracarboxylic acid tetrapotassium salt (PTAS) was used as a growth promoter to increase grain size. For the MoS_2 growth, 3 g of sulfur flakes were loaded upstream at the edge of the furnace. The SiO_2/Si substrate was placed face down over approximately 0.5 mg of solid MoO_3 and positioned at the center of the heating zone. For the WSe_2 growth, 2 g of selenium pellets were loaded upstream. An 8 mg of WO_3 and the SiO_2/Si substrate were positioned 30 cm and 35 cm downstream from the selenium, respectively. The system was pumped down to the base pressure before being raised to atmospheric pressure by Ar filling, followed by increasing the temperature to 750 – 880 °C under either pure Ar (for MoS_2 growth) or a mixed Ar + H_2 atmosphere (for WSe_2 growth). The furnace was held at optimum growth temperature for 10 – 40 min before cooling down to room temperature naturally.